Journal of Magnetic Resonance **146,** 169–180 (2000)
doi:10.1006/jmre.2000.2145, available online at http://www.idealibrary.com on IDEAL®

Two-Dimensional PFG NMR for Encoding Correlations of Position, Velocity, and Acceleration in Fluid Transport

Song-I Han, Siegfried Stapf, and Bernhard Blümich

Lehrstuhl für Makromolekulare Chemie and Magnetic Resonance Center MARC, RWTH Aachen, Worringerweg 1, D-52074 Aachen, Germany

E-mail: sstapf@erato.mc.rwth-aachen.de

Received February 14, 2000; revised June 6, 2000

A generalized approach to obtain two-dimensional maps of spatial particle coordinates and their derivatives with respect to time by PFG-NMR employing multiple gradient pulses is presented. A sequence of n magnetic field gradient pulses makes it possible, after independent stepping of each pulse and subsequent Fourier transformation, to plot the spin density distribution in coordinate space at n times and along the respective directions of the gradient pulses. In particular, two gradient pulses of effective area $\mathbf{k}_1$ and $\mathbf{k}_2$ separated by a time interval Δ lead to a plot of the combined two-time probability density, $W_2(\mathbf{r}_1, 0; \mathbf{r}_2, \Delta)$, to find a particle at a coordinate $\mathbf{r}_1$ at $t = 0$ and at $\mathbf{r}_2$ at $t = \Delta$. A conventional experiment for measuring transport properties by simultaneous stepping of the gradients under the condition $\mathbf{k}_1 = -\mathbf{k}_2$ is equivalent to a projection onto the secondary diagonal in the $[\mathbf{r}_1, \mathbf{r}_2]$ plot. The main diagonal represents an average position between the two timepoints $t = 0$ and $t = \Delta$, so that a rotation of the coordinate plot by an angle of 45° allows one to correlate the displacement $\mathbf{R} = \mathbf{r}_2 - \mathbf{r}_1$ with the averaged position $\mathbf{r}$ parallel to the gradient direction. While an average velocity during the time interval Δ can be defined as $\bar{v} = \mathbf{R}/\Delta$, an extension toward acceleration and higher order derivatives is straightforward by modification of the pulse sequence. We discuss this concept by application to flow through a circular and a narrowing pipe (confusor), respectively, the experimental results of which are compared to numerical simulations. © 2000 Academic Press

Key Words: **flow; position encoding; two-dimensional maps; correlation of motion; exchange spectroscopy.**

INTRODUCTION

In recent years, NMR investigations of transport processes have attracted considerable interest. Applications range from the monitoring of laminar and turbulent flow through simple geometries (*1–4*) to the characterization of flow in random, artificial, or natural porous systems (*5–14*). The techniques developed so far have mainly focused either on a purely statistical description of the fluid dispersion by obtaining the probability density of displacements, or propagator (*15*), averaged over a certain portion of the sample or on combining velocity encoding with imaging sequences to map average velocities with spatial resolution. More recently, these basic experiments have been extended to allow an analysis of correlations between displacements in different directions (*16–20*) or at successive times (*17, 21, 22*). In particular, the velocity exchange spectroscopy (VEXSY) concept (*23*) has been designed to visualize either the change of one velocity component between two separated time intervals or the displacement correlation function with respect to two successive time intervals (*24*). In this work, we introduce a PFG sequence, the purpose of which is to demonstrate positional changes at different times, and compare information derived from these measurements to results obtained by employing the VEXSY experiment. Both methods, and extensions thereof, are interpreted in terms of two-dimensional experiments to correlate averaged parameters of motion at successive times with each other and with their respective time derivatives.

THEORETICAL BACKGROUND

The principle of NMR imaging by phase encoding, and of NMR methods for determining transport processes such as coherent flow and random self-diffusion, is given by a spatial encoding of the positions of spin-bearing particles by imposing a space dependence of the magnetic field strength. If this space dependence is brought about by short magnetic field gradient pulses, during which particle motion can be neglected, the full spin density along the direction of the gradients at the time of their application can be obtained. Intensity and phase of the signal after a pulse sequence including a single gradient pulse, $\mathbf{G}_1$, are related to the spin density $P(\mathbf{r}_1)$ by

$$S(\mathbf{k}_1) = \int P(\mathbf{r}_1) e^{i2\pi \mathbf{k}_1 \mathbf{r}_1} \, d\mathbf{r}_1, \qquad [1]$$

where $\mathbf{k}_1 = (2\pi)^{-1}\gamma\delta\mathbf{G}_1$ is the effective wave vector of the gradient of duration δ, and γ is the gyromagnetic ratio.

The spin density $P(\mathbf{r}_1)$ along the direction of $\mathbf{r}_1$ can thus be obtained by stepping along the $\mathbf{k}_1$ axis followed by Fourier

1090-7807/00 $35.00

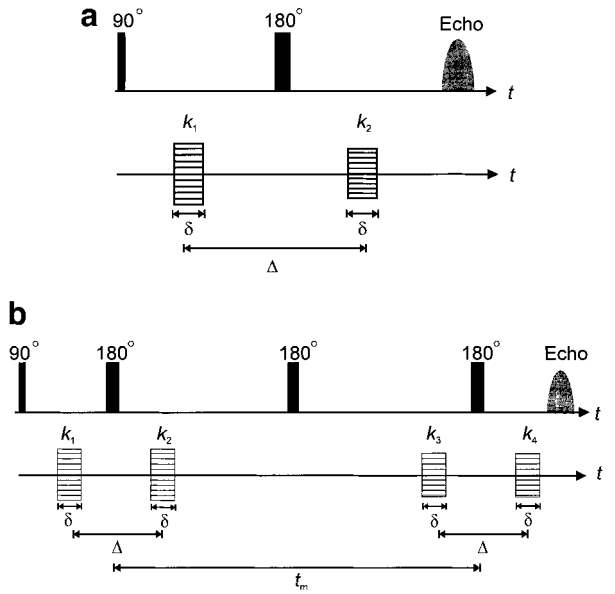

FIG. 1. (a) Spin-echo pulse sequence to encode positions at two times (POXSY). Both gradients of wave vector $\mathbf{k}_1$ and $\mathbf{k}_2$ are stepped independently of each other. (b) Spin-echo pulse sequence to encode displacements at two times (VEXSY). Both gradient pairs of wave vector $\mathbf{q}_1 = (\mathbf{k}_2 - \mathbf{k}_1)/2$ and $\mathbf{q}_2 = (\mathbf{k}_4 - \mathbf{k}_3)/2$ are stepped independently of each other.

transformation with respect to $\mathbf{k}_1$. The resolution is limited by the number of steps and by broadening due to motion occurring during the presence of the gradient pulse, δ, which can be approximated by $\langle \mathbf{r}^2 \rangle^{1/2} = \sqrt{2D\delta}$ for pure self-diffusion with a diffusion coefficient D, and by $v_{\max}\delta$ for flow with a maximum velocity $v_{\max}$.

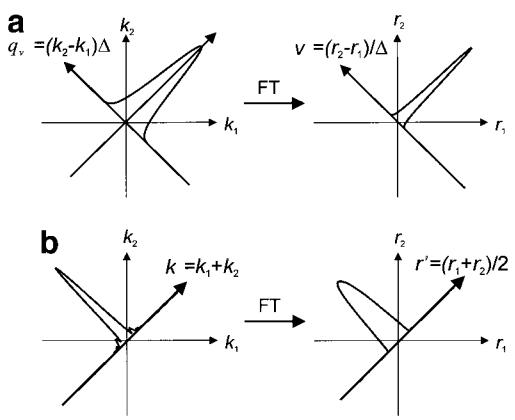

FIG. 2. Two-dimensional coordinate system for encoding by two pulsed gradients, $[\mathbf{k}_1, \mathbf{k}_2]$, and its Fourier conjugate in position space, $[\mathbf{r}_1, \mathbf{r}_2]$. (a) The secondary diagonals are sampled by stepping the gradients according to the condition $\mathbf{k}_1 = -\mathbf{k}_2$. The curves shown represent $\mathbf{q}$-space and $\boldsymbol{v}$-space data, respectively, for the example of unrestricted self-diffusion. (b) The main diagonals are sampled for stepping the gradients according to the condition $\mathbf{k}_1 = \mathbf{k}_2$. The curves shown represent $\mathbf{k}$-space and $\mathbf{r}$-space data, respectively, for the example of a water-filled cylindrical pipe.

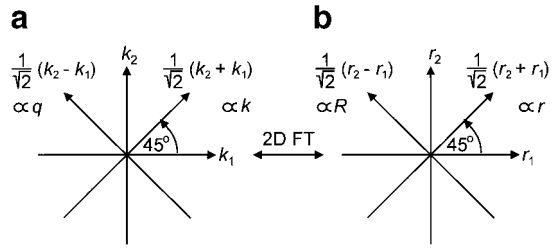

FIG. 3. Definition of $\mathbf{q}$ space in terms of the position exchange experiment (POXSY). (a) Initial and final positions are encoded by $\mathbf{k}_1$ and $\mathbf{k}_2$ in the narrow gradient pulse approximation. The transformation to a coordinate system where the difference wave number $\mathbf{q}$ defines one of the axes corresponds to a right-handed 45° rotation of the coordinate system. The perpendicular variable is proportional to the wave number $\mathbf{k}$, which encodes position. (b) Two-dimensional Fourier transformation of such a position-exchange data set produces the displacement coordinate $\mathbf{R}$ in a coordinate frame rotated by 45° on one axis and the averaged positional coordinate $\mathbf{r}$ on the other axis.

A second pulse of identical intensity but possessing the opposite effective direction and being applied after a time interval Δ allows the determination of the distribution of displacements relative to the starting position of each spin. Formally, this corresponds to performing two space-encoding experiments which are linked to each other by the condition $\mathbf{k}_1 = -\mathbf{k}_2$,

$$S(\mathbf{q}) = \int\int P(\mathbf{r}_1)\, P(\mathbf{r}_1|\mathbf{r}_2,\, \Delta) e^{i2\pi\mathbf{q}(\mathbf{r}_2 - \mathbf{r}_1)}\, d\mathbf{r}_1\, d\mathbf{r}_2$$

$$= \int P(\mathbf{R}) e^{i2\pi\mathbf{q}\mathbf{R}} d\mathbf{R}, \qquad [2]$$

where $\mathbf{R} = \mathbf{r}_2 - \mathbf{r}_1$ is the displacement during Δ and its Fourier conjugate is denoted by $\mathbf{q}$ in accordance with the literature (*25*). $P(\mathbf{r}_1)$ is the probability density for starting positions at

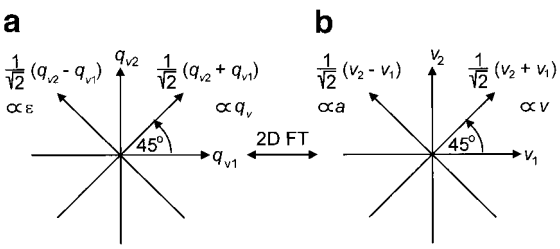

FIG. 4. Definition of $\boldsymbol{\epsilon}$ space in terms of the velocity exchange experiment (VEXSY). (a) Initial and final velocities are encoded by $\mathbf{q}_1$ and $\mathbf{q}_2$ in the approximation of short Δ. The transformation to a coordinate system where the difference wave number $\boldsymbol{\epsilon}$ defines one of the axes corresponds to a right-handed 45° rotation of the coordinate system. The perpendicular variable is proportional to the wave number $\mathbf{q}$, which encodes displacement. (b) Two-dimensional Fourier transformation of such a velocity-exchange data set produces the acceleration coordinate $\mathbf{a}$ in a coordinate frame rotated by 45° on one axis and the averaged velocity coordinate $\boldsymbol{v}$ on the other axis.

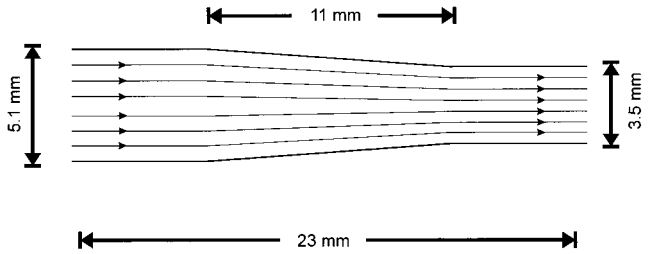

FIG. 5. Dimensions of the sample cell for experiments on flow through a narrowing pipe. Streamlines are drawn schematically. The long bar (23 mm) represents the sensitive volume of the resonator coil.

$t = 0$, while $P(\mathbf{r}_1|\mathbf{r}_2, \Delta)$ is the conditional probability for displacements from $\mathbf{r}_1$ to $\mathbf{r}_2$ in time Δ (*25*). Under these conditions, the information about the starting positions is lost and only the distribution of displacements along the axis of the applied magnetic field gradients is retained. This so-called propagator $P(\mathbf{R})$ can be obtained directly by Fourier transformation of $S(\mathbf{q})$ with respect to $\mathbf{q}$.

However, the same experiment may also be performed with both gradients being varied independently of each other. In Fig. 1a, one possible realization of this experiment is shown. Depending on parameters such as field homogeneity and relaxation times, either a gradient echo, spin echo, or stimulated echo variant can be chosen. Because the pulse sequence contains two pulsed gradients $\mathbf{G}_1$ and $\mathbf{G}_2$, with $\mathbf{G}_1$ parallel to $\mathbf{G}_2$ in this case, corresponding to the wave vectors $\mathbf{k}_1$ and $\mathbf{k}_2$, a coordinate system defined by $\mathbf{k}_1$ and $\mathbf{k}_2$ can be introduced. The $\mathbf{k}$-space intensity plot is now defined in the general way as

$$S(\mathbf{k}_1, \mathbf{k}_2) = \int\int P(\mathbf{r}_1)\, P(\mathbf{r}_1|\mathbf{r}_2, \Delta) e^{i2\pi\mathbf{k}_1\mathbf{r}_1} e^{i2\pi\mathbf{k}_2\mathbf{r}_2}\, d\mathbf{r}_1\, d\mathbf{r}_2$$

$$= \int\int W_2(\mathbf{r}_1, 0; \mathbf{r}_2, \Delta) e^{i2\pi\mathbf{k}_1\mathbf{r}_1} e^{i2\pi\mathbf{k}_2\mathbf{r}_2}\, d\mathbf{r}_1\, d\mathbf{r}_2. \quad [3]$$

Here we have renamed the Fourier conjugate of the $\mathbf{k}$-space intensity function, $P(\mathbf{r}_1)\, P(\mathbf{r}_1|\mathbf{r}_2, \Delta)$, as the two-time probability density $W_2(\mathbf{r}_1, 0; \mathbf{r}_2, \Delta)$ to find a particle at position $\mathbf{r}_1$ at $t = 0$ *and* at position $\mathbf{r}_2$ at $t = \Delta$. This generalized approach allows one to map the change of position of particles between $t = 0$ and $t = \Delta$, and therefore shall be denoted by the term *po*sition e*x*change spectroscop*y* (POXSY). Note that due to the phase-encoding scheme, the chemical information of the echo is kept in principle and allows the spectral analysis of multicomponent systems simultaneously, thereby supplying an additional dimension to the experiment.

The displacement spectrum obtained from a one-dimensional PFG experiment is still contained in the result of the full POXSY plot. The condition $\mathbf{k}_1 = -\mathbf{k}_2$ is equivalent to a stepping along the secondary diagonal in the $[\mathbf{k}_1, \mathbf{k}_2]$ space. In the Fourier conjugate space, the displacement spectrum is described by a projection onto the secondary diagonal, $\mathbf{r}_2 - \mathbf{r}_1$. Given that the quotient of the displacement $\mathbf{R}$ and the evolution time Δ defines an average velocity $\bar{v}$, the secondary diagonal can also be understood as a velocity axis (see Fig. 2a). On the

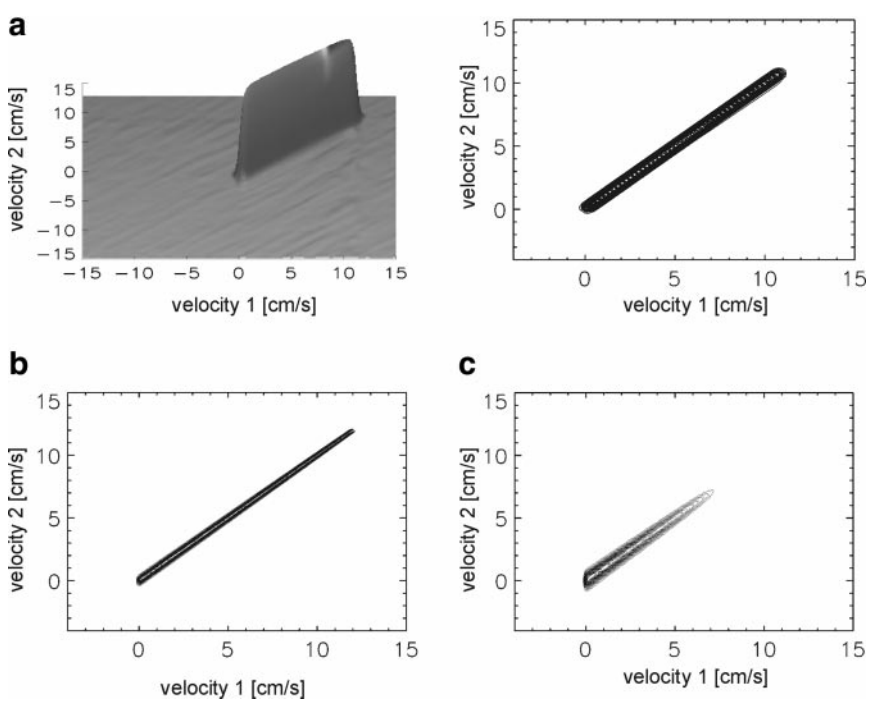

FIG. 6. Flow of water at $\overline{v_z} = 6$ cm/s through a circular pipe of 4.8 mm inner diameter. Velocities during the first and second interval are shown on the $v_{z,1}$ and $v_{z,2}$ axis, respectively. (a) Two-dimensional VEXSY experiment, $\Delta = 23.5$ ms, $t_m = 60$ ms. (b) Simulation, same parameters as in (a). (c) Simulation, same parameters as in (b) except $t_m = 300$ ms.

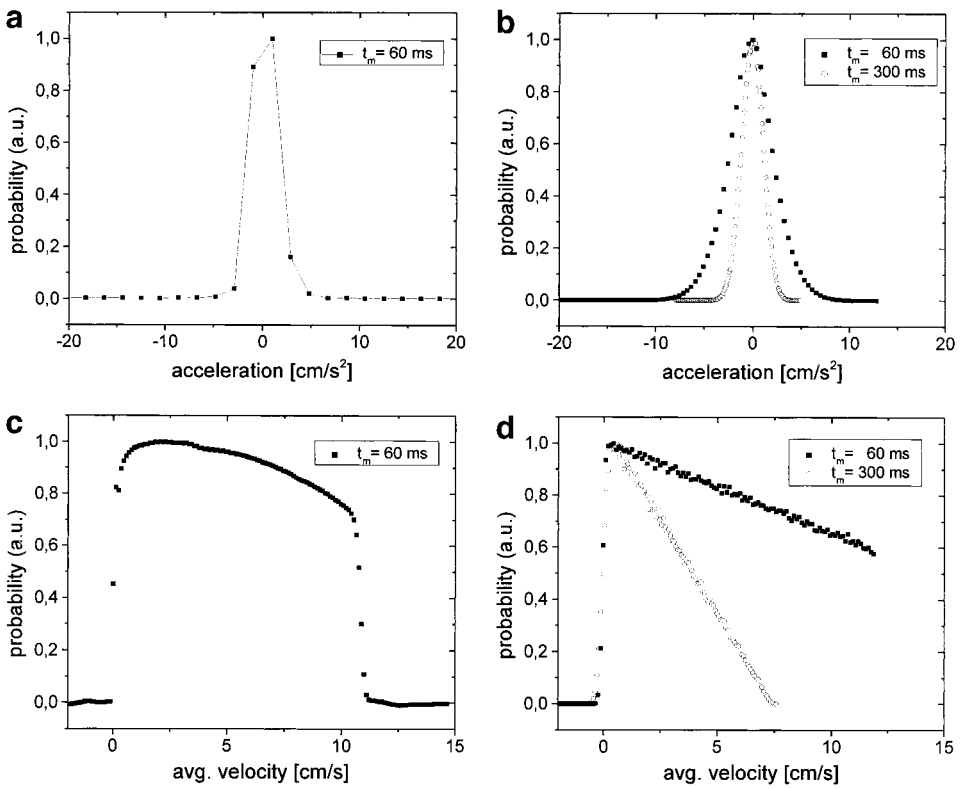

FIG. 7. (a) Projection onto the secondary diagonal for the experimental data of Fig. 6a, representing the distribution of accelerations, $P(a_z)$. (b) As in (a) but for simulated data. (c) Projection onto the main diagonal for the experimental data of Fig. 6a, representing the distribution of average velocities, $P(v_z)$. (d) As in (c) but for simulated data.

other hand, application of two gradient pulses of identical effective wave vectors, $\mathbf{k}_1 = \mathbf{k}_2$, corresponds to an encoding of the average position between both times, $t = 0$ and $t = \Delta$, which is drawn along the $[\mathbf{r}_1, \mathbf{r}_2]$ main diagonal (see Fig. 2b). Because of this interpretation of the diagonals in the two-dimensional position space, a 45° rotation of the coordinate system in the mathematically positive sense provides the correlation between position and velocity (*26*, *27*) as schematically sketched in Fig. 3. Note that for a direct comparison of dimensions, the axes are transformed according to $\mathbf{R}' = (\mathbf{r}_2 - \mathbf{r}_1)/\sqrt{2}$ and $\mathbf{r}' = (\mathbf{r}_1 + \mathbf{r}_2)/\sqrt{2}$, respectively (*26*).

The scheme can be extended one step further from exchange in $\mathbf{k}$ space to exchange in $\mathbf{q}$ space. The pulse sequence now consists of two *pairs* of gradient pulses, $\mathbf{k}_1 = -\mathbf{k}_2$ and $\mathbf{k}_3 = -\mathbf{k}_4$, encoding displacements during a time interval Δ and being separated by a mixing time t_m (see Fig. 1b). For Δ values short compared to the characteristic velocity fluctuation times in the system, each gradient pair measures the molecular velocity distribution, and the sequence is identical to the *v*elocity *ex*change *s*pectroscop*y* (VEXSY) experiment which was presented by Callaghan and Manz (*23*). In full analogy to the case described above, and renaming the wave vectors as $\mathbf{q}_1 = (\mathbf{k}_2 - \mathbf{k}_1)/2$ and $\mathbf{q}_2 = (\mathbf{k}_4 - \mathbf{k}_3)/2$, one obtains a two-dimensional $[\mathbf{q}_1, \mathbf{q}_2]$ space and its Fourier conjugate, the $[\mathbf{R}_1, \mathbf{R}_2]$ space of displacements which is equivalent to the average velocities $[v_1, v_2]$ for equal encoding times Δ between both gradient pairs:

$$
\begin{aligned}
S(\mathbf{q}_1, \mathbf{q}_2) &= \int\int P(\mathbf{R}_1)\, P(\mathbf{R}_1|\mathbf{R}_2, t_\mathrm{m}) e^{i2\pi\mathbf{q}_1\mathbf{R}_1} e^{i2\pi\mathbf{q}_2\mathbf{R}_2}\, d\mathbf{R}_1\, d\mathbf{R}_2 \\
&= \int\int W_2(\mathbf{R}_1, 0; \mathbf{R}_2, t_\mathrm{m}) e^{i2\pi\mathbf{q}_1\mathbf{R}_1} e^{i2\pi\mathbf{q}_2\mathbf{R}_2}\, d\mathbf{R}_1\, d\mathbf{R}_2 \\
&= \int\int W_2(v_1, 0; v_2, t_\mathrm{m}) e^{i2\pi\mathbf{q}_{v,1}v_1} e^{i2\pi\mathbf{q}_{v,2}v_2}\, dv_1\, dv_2.
\end{aligned}
\qquad [4]
$$

Here, we have replaced $\mathbf{q}_i$ by $\mathbf{q}_{v,i} = \mathbf{q}_i\Delta$ (*26*) to allow a direct representation of velocities, and $W_2(v_1, 0; v_2, t_\mathrm{m})$ now describes the two-time probability density to find a particle with velocity v_1 at $t = 0$ and with velocity v_2 at $t = t_\mathrm{m}$, where both "time points" are given by averaging over the encoding time Δ.

Again, the diagonals can be interpreted in a similar way as that in the positional exchange experiment. The main diagonal in $\mathbf{q}_v$ space, given by $\mathbf{q}_{v,1} = \mathbf{q}_{v,2}$, encodes the average velocity distribution during the mixing time t_m. The secondary diago-

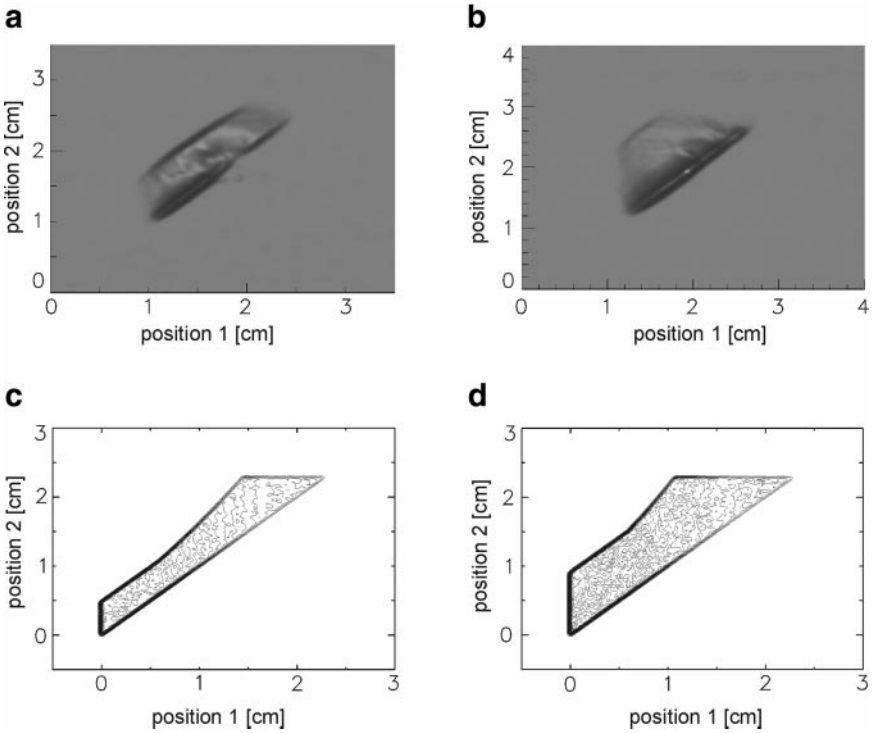

FIG. 8. Position exchange spectroscopy (POXSY) experiment for flow of water through a narrowing pipe (confusor) of inner diameters 5.1 to 3.5 mm. (a) Two-dimensional position plot from experimental data for $\Delta = 17$ ms and (b) 32 ms. (c) Same as (a) but for simulated data. (d) Same as (b) but for simulated data.

nal, on the other hand, fulfilling the condition $\mathbf{q}_{v,1} = -\mathbf{q}_{v,2}$, corresponds to the one-dimensional double PGSE experiment of Callaghan *et al.* (*24*) and probes velocity changes. If the position of a particle is expanded into a Taylor series,

$$\mathbf{r}(t) = \mathbf{r} + vt + \frac{1}{2}\,\mathbf{a}t^2 + \cdots, \qquad [5]$$

one can likewise denote the phase shift as a function of the magnetic field gradient by (*28*)

$$\phi = \phi_0 + \frac{\mathbf{kr}}{2\pi} + \frac{\mathbf{q}_v v}{2\pi} + \frac{\boldsymbol{\epsilon}\mathbf{a}}{2\pi} + \cdots, \qquad [6]$$

which defines the Fourier conjugate to acceleration, $\boldsymbol{\epsilon}$ (*26, 27*). It is this variable which is plotted along the secondary diagonal.

On the other hand, the main diagonal of the matrix $W_2(v_1, 0; v_2, t_m)$ now represents the velocity averaged over t_m, and the secondary diagonal the distribution of velocity changes, which in the finite difference approximation defines a distribution of accelerations, $P(\mathbf{a})$ with $\mathbf{a} = (v_2 - v_1)/\Delta$. A 45° rotation of the coordinate system now provides the correlation between velocity and acceleration (*26, 27*) (see Fig. 4).

EXPERIMENTS AND SIMULATIONS

All experiments were performed using a Bruker 300 MHz DMX spectrometer with a horizontal bore magnet of 200 mm accessible diameter, employing the pulse sequences shown in Fig. 1. The intensity of the gradient pulses and the gradient pulse pairs, respectively, was varied in 151 × 151 steps covering the range $\pm\mathbf{k}_{i,\max}$ and $\pm\mathbf{q}_{i,\max}$. The signal was accumulated using a four-phase cycle, resulting in total durations of the experiments of typically 7 h.

The behavior of fluid under laminar flow conditions was investigated using water (doped with $CuSO_4$ to reduce T_1 to the range of 100–200 ms) flowing in a hydraulically smooth PMMA (polymethylmethacrylate) pipe of 4.8 mm inner diameter. The length of the inlet was about 50 cm to establish stationary flow conditions. A constant volume flow rate in the rate 50–150 ml/min, corresponding to average flow velocities of 5 to 15 cm/s, was maintained using an Ismatec Reglo-Z pump (Ismatec Laboratoriumstechnik GmbH, Wertheim-Mondfeld, Germany).

The experimental setup to measure the flow of water through a narrowing pipe (confusor) is shown schematically in Fig. 5. To allow for shorter repetition times and a higher resolution necessary for performing a POXSY-type experiment, the relaxation time T_1 has been reduced by adding $CuSO_4$ to about 50 ms. An Ismatec BVP-Z pump was employed to maintain a constant volume flow rate of 170 ml/min, corresponding to an

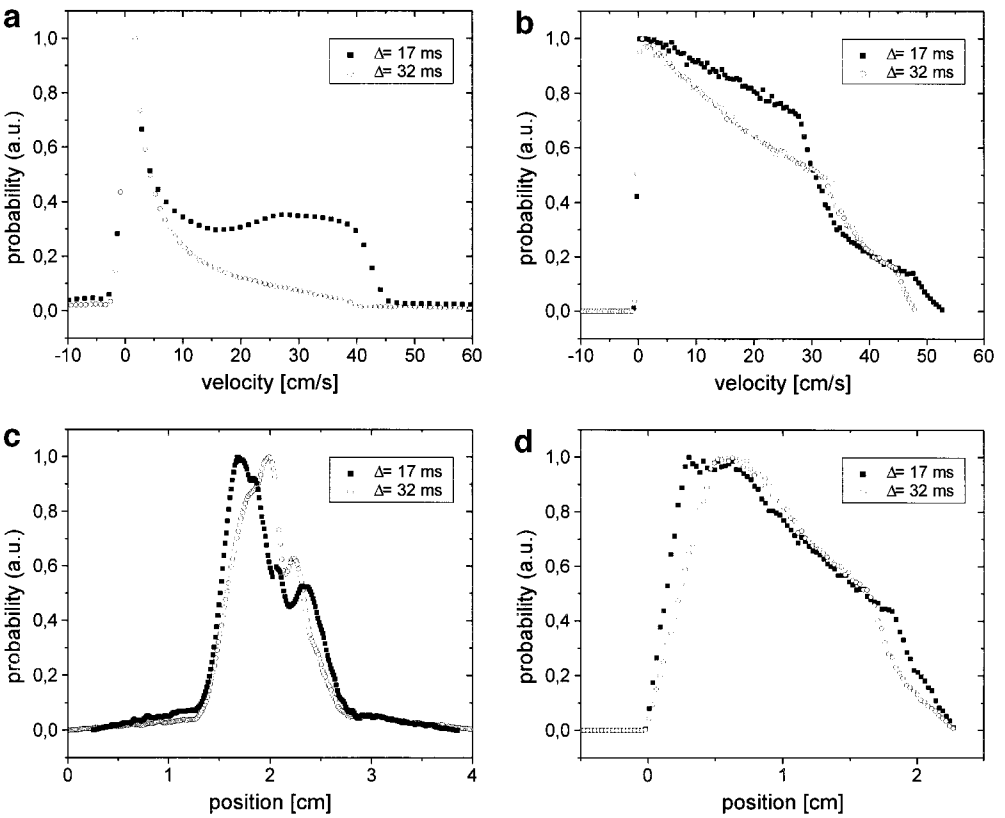

FIG. 9. (a) Projection onto the secondary diagonal for the experimental data of Fig. 8, representing the distribution of velocities. (b) As in (a) but for simulated data. (c) Projection onto the main diagonal for the experimental data of Fig. 8, representing the distribution of average positions parallel to the direction of the applied magnetic field gradient pulses. (d) As in (c) but for simulated data.

average flow velocity of 14 cm/s in the wide region of the pipe and 30 cm/s in the narrow region. In the POXSY experiment, Δ was varied between 17 and 32 ms. To obtain the velocity exchange spectrum (VEXSY), Δ was fixed to 3.0 ms and t_m was varied in the range 17 to 43 ms.

To achieve a qualitative understanding of the experimental results, numerical simulations were performed for the case of flow through a straight, cylindrical pipe and through a confusor with geometrical conditions matching those in the experimental setup. Typically 10^6 particles were allowed to undergo flow, assuming laminar conditions throughout the sample geometry, while radial and axial self-diffusion steps were introduced into each evolution interval. The velocity distribution in the cone of the second sets of simulations was obtained by mapping the parabolic velocity profile onto the local pipe diameter, and edge effects such as the development of vortices were not considered. Particles leaving the "field of view," which was adjusted to the true conditions in the resonator, were removed from the statistics.

RESULTS AND DISCUSSION

Laminar flow conditions are observed for Newtonian fluids in straight cylindrical pipes in the case of low velocities. The transition from laminar to turbulent flow is characterized by the Reynolds number which is defined as the ratio of inertial and viscous forces,

$$\mathrm{Re} = \frac{\bar{v}L}{\nu}, \qquad [7]$$

where $\bar{v}$ is the average velocity magnitude, ν is the kinematic viscosity of the fluid, and L denotes some characteristic length scale in the system such as the tube diameter. Below a critical Reynolds number of $\mathrm{Re}_c \approx 2300$ (*29*), laminar flow is observed in the presence of hydraulically smooth walls. If self-diffusion is neglected, the velocity of a fluid particle is a function of its radial distance r from the center of the pipe of radius r_0,

$$v(r) = v_{\max}\left[1 - \left(\frac{r}{r_0}\right)^2\right], \qquad [8]$$

where $v_{\max} = 2\bar{v}$. This parabolic dependence can be visualized by appropriate combinations of velocity-encoding and imaging techniques (see, e.g., (*30*, *31*)). The probability density to find a particle with a certain velocity v is then given by an integral of $v(r)$ over the sample volume. This distribution function is

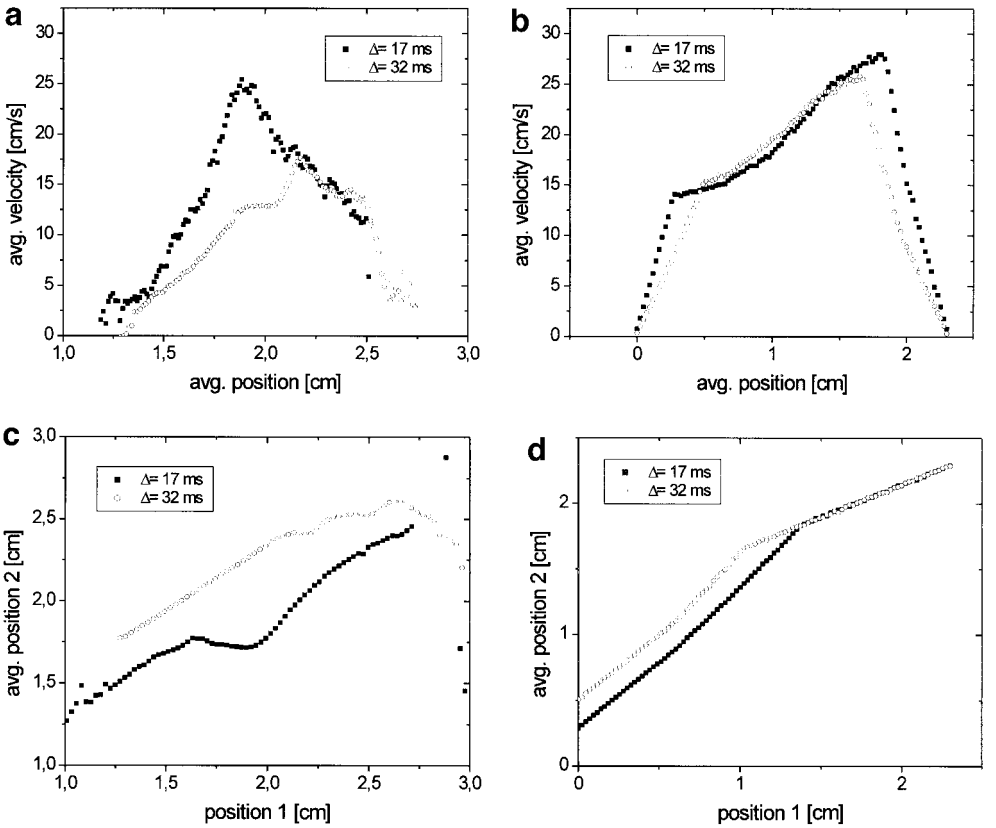

FIG. 10. (a) Average velocity as a function of the average position in the confusor (experimental data). (b) As in (a) but for simulated data. (c) Average position $\langle z_2 \rangle$ as a function of starting position z_1 (experimental data). (d) As in (c) but for simulated data.

equivalent to the probability density of displacements, the so-called propagator (*15*), and possesses a box-like shape between $R = 0$ and $R = v_{max}\Delta$. Random self-diffusion during Δ leads to a mixing of particles between streamlines so that the box-like shape eventually evolves over time as the diffusion length becomes comparable to the pipe dimensions (*32*). Under turbulent conditions, the propagator deviates from a rectangular shape, and the probability increases to find particles with high velocities (*31*).

To demonstrate the feasibility of performing exchange experiments on laminar flow, the Reynolds number for flow of water in a cylindrical pipe has been chosen to be in the range 240 to 720 to remain well below the laminar/turbulent transition at $Re_c \approx 2300$. The VEXSY scheme allows one to correlate velocity components in two encoding intervals separated by a mixing time t_m. One example for the two-time probability density function $W_2(v_{z,1}, 0; v_{z,2}, t_m)$ is shown in Fig. 6a for $\Delta = 23.5$ ms, $t_m = 60$ ms, with an average velocity $\overline{v_z} = 6$ cm/s along the flow axis corresponding to Re = 290. The experimental data are compared to simulated particle distribution plots in Fig. 6b. For the chosen parameters, Taylor dispersion is still negligible and the experimentally obtained propagator is of apparently perfect box-shape. However, at a fivefold increased mixing time ($t_m = 300$ ms) (see Fig. 6c), it can be seen that the largest contributions to exchange are observed at the lowest velocities. In this region near the pipe wall, the velocity gradient $\partial v_z/\partial r$ is largest and a given radial displacement due to self-diffusion leads to a maximum change in velocities. Projections onto the secondary and the main diagonal, respectively, reproduce the distribution of average acceleration (Figs. 7a and 7b) and average velocity (Figs. 7c and 7d) in analogy to an equivalent one-dimensional experiment with $q_{z,1}$, $q_{z,2}$ being varied simultaneously.

The experimental distribution of accelerations, $P(a_z)$, is in agreement with the simulated data; however, the experimental data suffer from a somewhat limited resolution. It can be seen that for increasing times, the average acceleration decreases, which is due to the fact that the velocity change Δv_z due to self-diffusion scales with $t^{1/2}$ while the acceleration scales with $\Delta v_z t^{-1}$.

The distribution of average velocities, which is plotted along the main diagonal in the $[v_{z,1}, v_{z,2}]$ space, is characterized in principle by a constant between 0 and v_{max}. The decrease in intensity toward large velocities is due to the fraction of particles which have left the sensitive volume of the resonator during the mixing time (see Fig. 7c). This effect has been considered in the simulations, where a sensitive volume of 23 mm length has been set in accordance with results from one-dimensional spin-density profiles taken along the direction of

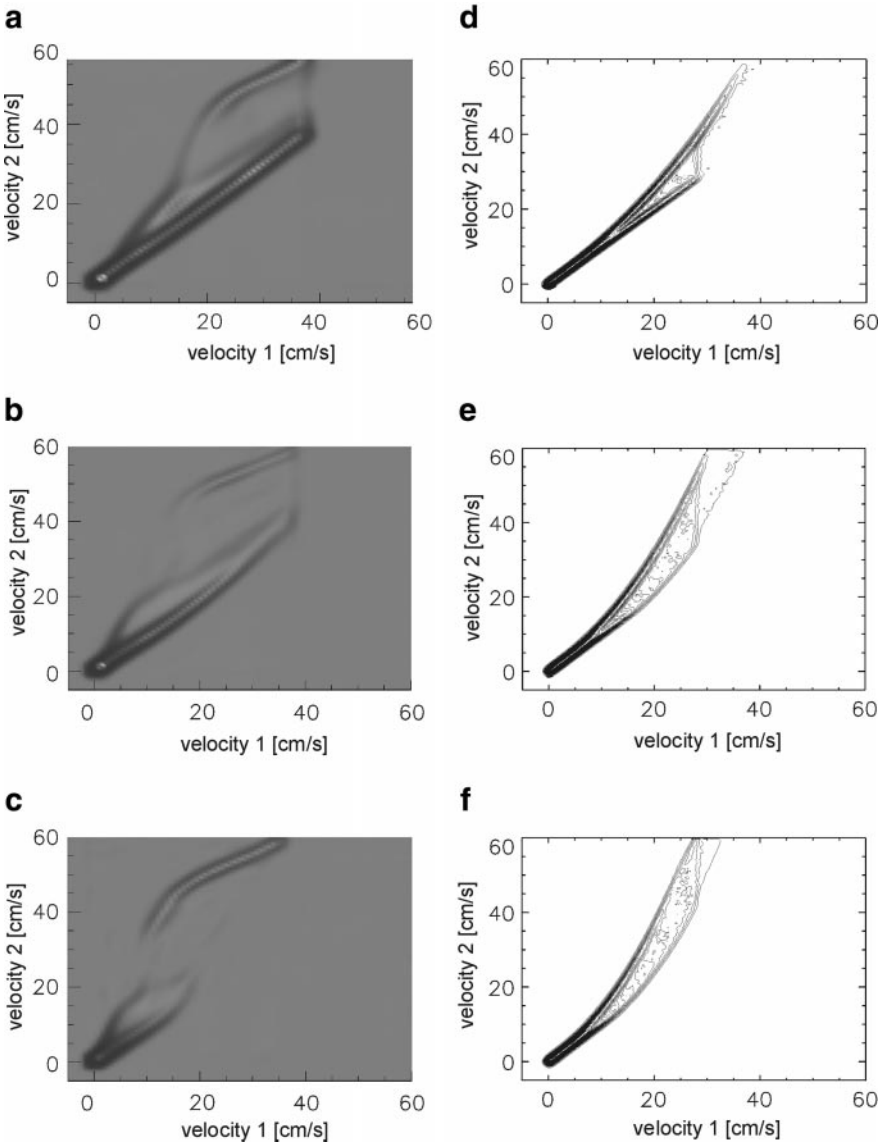

FIG. 11. Velocity exchange spectroscopy (VEXSY) experiment for flow of water through a narrowing pipe (confusor) of inner diameters 5.1 to 3.5 mm. Two-dimensional velocity plot for experimental data with (a) $t_m = 17$ ms, (b) 32 ms, and (c) 43 ms. (d–f) As in (a–c) but for simulated data.

the coil. In Fig. 7d, this outflow effect becomes much more pronounced for $t_m = 300$ ms where the average displacement is already 1.8 cm.

As an appropriate test sample for performing a POXSY experiment, the purpose of which is to correlate particle positions at two successive times with each other and to provide a link between the velocity and the position of a particle, we have chosen a glass confusor, consisting of long cylindrical portions of 5.1 and 3.5 mm inner diameters, respectively, on either side that are joined by a narrowing conical section located completely within the sensitive volume of the resonator coil (see Fig. 5). Particle velocities will then be largest in the narrow cylindrical part, with intermediate values found in the transition region. The result of a POXSY experiment with two gradient pulses in the direction z of the flow axis stepped independently is shown in Figs. 8a and 8b for two different encoding times Δ of 17 and 32 ms. The flow rate of 170 ml/min corresponds to average velocities of 14 cm/s in the wide region and 30 cm/s in the narrow region of the confusor; the Reynolds numbers in these sections are 710 and 1050. The results agree reasonably well with the simulated data (see Figs. 8c and 8d), the main difference being a more pronounced main diagonal $z_1 = z_2$ representing static spins.

The plots of the function $W_2(z_1, 0; z_2, \Delta)$ presented in Fig. 8 can be understood as follows: the wider part of the sample is located in the lower left corner of the plot and is indicated by a higher number of spins because the signal is obtained from an integration of the spin density over the cross section of the

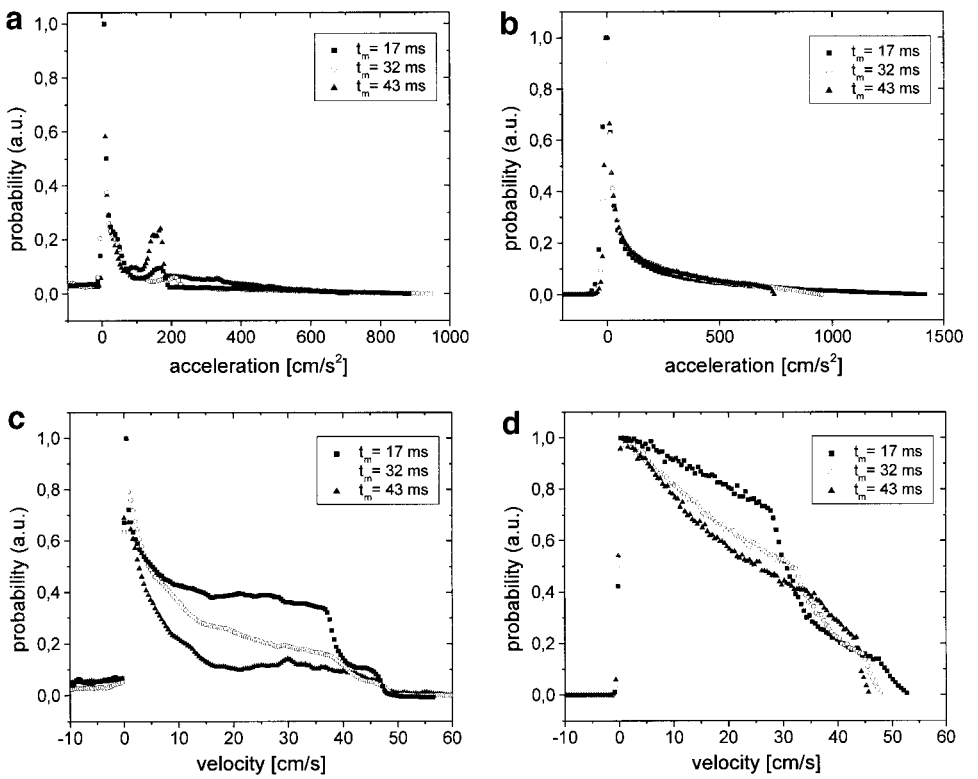

FIG. 12. (a) Projection onto the secondary diagonal for the experimental data of Fig. 11, representing the distribution of accelerations during t_m. (b) As in (a) but for simulated data. (c) Projection onto the main diagonal for the experimental data of Fig. 11, representing the distribution of average velocities. (d) As in (c) but for simulated data.

pipe. Here, the spread in the direction along the secondary diagonal is less pronounced, because particles in this region possess smaller velocities on average and the change in position during the given interval Δ is smaller than that in the narrow region of the sample. A larger spread in the narrow portion of the sample is prevented by the outflow effect.

Projections onto the secondary and the main diagonal are presented in Figs. 9a–9d. The distribution of averaged velocities (see Figs. 9a and 9b) is described by a decreasing probability of finding large velocities. This observation becomes more pronounced for larger Δ. While a smaller number of particles is contained in the narrow cylindrical portion of the confusor, these are also more likely to leave the volume of the resonator. The same effect affects the determination of the average position along the flow direction (see Figs. 9c and 9d). In the absence of outflow, the main diagonal would represent a profile over the sample smeared by flow during the interval Δ. As was discussed above, the projections shown in Fig. 9 are identical to the results of corresponding 1-d PFG experiments employing pairs of gradients of opposite and equal sign, respectively.

The two-dimensional data set can now be employed to compute two different kinds of correlations. First, as outlined under Theoretical Background, the average position *difference* for each average position can be calculated in order to provide a correlation between position and velocity. This is done by determining the weighted mean value of $z_2 - z_1$ for any given $\langle z \rangle = \frac{1}{2}(z_1 + z_2)$. The result is shown in Figs. 10a and 10b. In general, large (average) positions are linked to larger velocities, because they correspond to particles in the narrow part of the tube. Particles which remain near the right edge of the sample, and consequentially have large average positions, must necessarily possess smaller velocities or do not contribute to the signal at $t = \Delta$ anymore, which determine the general shape of the position/velocity correlation function.

On the other hand, returning to the main axes coordinate system, the average of z_2 can be computed for any starting position z_1. In this case, one expects the difference between $\langle z_2 \rangle$ and z_1 to be given by the product of average flow velocity and encoding time, Δ. This is indeed the case as can be seen in Figs. 10c and 10d.

For all data discussed above, the agreement between experiment and simulation is mostly qualitative only. However, in the interpretation of the POXSY experiment, some obvious restrictions must be considered. First, the change in position during Δ must be small compared to the sample size if the averaged position during Δ, which is obtained from the projection onto the main diagonal, shall still bear a resemblance to the profile of the sample. On the other hand, small displacements during Δ necessitate sufficient resolution in **k** space

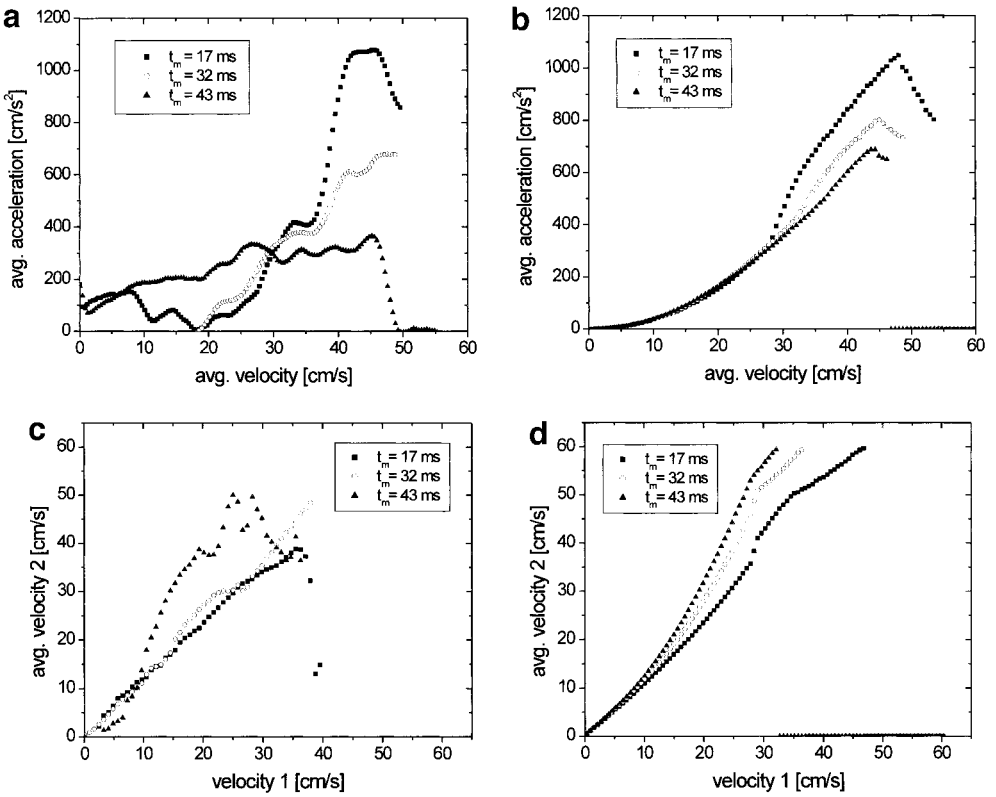

FIG. 13. (a) Average acceleration as a function of the average velocity in the confusor (experimental data). (b) As in (a) but for simulated data. (c) Average velocity $\langle v_{z,2} \rangle$ as a function of initial velocity $v_{z,1}$ (experimental data). (d) As in (c) but for simulated data.

while at the same time, the field of view must match the volume of interest of the sample. Furthermore, long experimental times allow the fastest particles to leave the sensitive volume of the resonator, which in turn falsifies the displacement statistics. A perfect match of the simulations to the experimental setup, taking into consideration the sensitivity distribution and edge effects of the resonator, has not been attempted. We believe that one major reason for the distorted and somewhat shortened shape of the sample image can be attributed to imperfect excitation and sensitivity at both edges of the resonator. It must also be noted that due to the nature of the double phase encoding, the presented sequence is particularly sensitive to B_0 and B_1 field inhomogeneities. A further disturbing influence of deviations from laminar flow is briefly addressed below.

It should be noted that an established method to obtain information about relations between position and velocity is given by velocity imaging, one realization of which involves pure phase encoding by a single gradient pulse (**k**, encoding position) followed by a pair of gradient pulses (**q**, encoding velocity). The main difference between both methods lies in the fact that velocity imaging attempts to sample the space-dependent velocity directly and thus relies on short separations between the **k** and **q** encoding steps. POXSY, on the other hand, provides an indirect measure of velocity via the sampling of position information at two successive times, the separation Δ representing a further variable which normally is not of interest in a velocity imaging experiment of the type described.

Under conditions identical to those in the POXSY experiment described above, we have performed VEXSY experiments where the mixing time t_m has been varied between 17 and 43 ms. The full two-dimensional plots of $W_2(v_{z,1}, 0; v_{z,2}, t_m)$ are shown in Figs. 11a–11c for the experimental and in Figs. 11d–11f for the simulated data. The results can be understood as follows: the diagonal $v_{z,1} = v_{z,2}$ represents particles which have not changed their velocity considerably during t_m. As even for the longest mixing time of 43 ms, the rms displacement for self-diffusion is on the order of 15 μm and therefore much smaller than the pipe diameters; a change of velocities is mostly brought about by crossing the region of variable tube radius and not by radial diffusion. The diagonal $v_{z,1} = v_{z,2}$ is therefore produced by those particles that have remained in either the wide or the narrow cylindrical portion of the sample. With increasing mixing time, those particles that possess the highest velocities at $t = 0$ have disappeared from the sensitive volume of the resonator so that the highest velocities do not occur anymore along the $v_{z,1}$ axis, and the diagonal $v_{z,1} = v_{z,2}$ appears shortened. A second ridge, which appears to the upper left end of the plot, stems from particles that have not changed their relative radial distance r/r_0 and

therefore experience a velocity change to $(5.1/3.5)^2 = 2.1$ times their starting value. The curved left part in the VEXSY plot is produced by those particles that have not fully crossed the transition regime and therefore have not experienced the full increase in velocity of a factor of 2.1.

The simulations assume that the undisturbed streamlines indicated in Fig. 5 represent the true situation. At the velocities and Reynolds numbers chosen for this experiment, this is not likely to be the case; the presence of regions with nonlaminar flow or vortices cannot be excluded. The deviation of the secondary ridge from a straight line in the experimental data might be the consequence of these imperfections. Moreover, a well-pronounced ridge at large $v_{z,2}$ appears in the experimental data, which follows the approximate relation $v_{z,2} = 0.75\ v_{z,1} + \text{const}$ and which becomes more evident with increasing mixing time.

In Fig. 12, the projections onto the diagonals for the VEXSY data are presented. The secondary diagonal (Figs. 12a and 12b) gives a measure for the change of velocities during this mixing time t_m. Given that the largest acceleration is experienced only by those particles that cross the conical part of the confusor while flowing near the center of the tube, this maximum acceleration is found to occur with a small relative probability, while the majority of the particles encounter only small velocity changes. The occurrence of a strong peak around 150 cm/s^2 in the experimental data reflects the secondary ridge in the two-dimensional VEXSY plot mentioned above and possibly is a consequence of nonlaminar flow conditions in the confusor.

The distribution of average velocities, as shown by projections onto the main diagonal (Figs. 12c and 12d), is dominated by a decrease of the probability of high velocities toward increasing t_m, again a consequence of the outflow effect. A qualitative agreement between experiment and simulation can be found.

In analogy to the analysis discussed for the POXSY experiment, the correlation between velocity change (corresponding to average acceleration averaged over t_m) and average velocity is demonstrated in Figs. 13a and 13b. Generally, large velocities are correlated with large average accelerations because only fast particles are able to cross the conical portion of the confusor within t_m and therefore experience a large change in velocity. This is not the case for the fastest particles within the narrow cylinder as their velocity remains essentially constant, and they are most likely to leave the resonator with increasing mixing time.

The second correlation that can be computed from the two-time function $W_2(v_{z,1}, 0; v_{z,2}, t_m)$ describes the average velocity $\langle v_{z,2} \rangle$ at time t_m as a function of the initial velocity, $v_{z,1}$. In Figs. 13c and 13d, experimental and simulated data again correspond qualitatively, with deviations occurring mainly at high velocities. As expected, $\langle v_{z,2} \rangle > v_{z,1}$ with the difference increasing with t_m and toward larger values of $v_{z,1}$. This observation is in accordance with the correlation observed between acceleration and average velocity, but the time average is now replaced by an ensemble average so that both informations can be regarded as being complementary.

In summary, the results obtained from two-dimensional POXSY and VEXSY experiments can qualitatively be reproduced with simple numerical simulations, which make it possible to explain the main features of the relationships of the measured quantities' position, velocity, and acceleration. Deviations between experiment and simulation indicate the high sensitivity of the data to the flow processes in the chosen geometry. Even taking the experimental restrictions discussed above into account, these differences cannot fully be attributed to experimental errors but rather are due to the simplicity of the model or the deviations of the actual experimental conditions from those used for performing the simulations. In particular, the assumption of laminar flow within the confusor as outlined above cannot be expected to reflect the real situation.

For more complicated situations, such as flow through complex geometries like narrow blood vessels and porous media, where simple simulations might not be readily available, the experimental methods and their interpretation with respect to correlations that have been presented in this work might represent a valuable tool for the understanding of flow processes in applications of technical and biomedical importance. An extension toward higher order time derivatives of motion seems feasible, as well as a generalization including more than two encoding steps. In all applications, some care must be taken in order to avoid misinterpretations of the obtained quantities; e.g., the computation of velocity or acceleration from statistical processes such as random self-diffusion or dispersion in fluid flow through porous media might not be the appropriate description of the problem.

CONCLUSIONS

We have presented a generalized approach to understand and explain basic NMR experiments to encode position, velocity, and acceleration. A pulsed field gradient experiment consisting of two gradient pulses encodes position at two different times and thus can be expressed as a means of performing position exchange spectroscopy. The two-dimensional data set can be transformed into a coordinate frame which correlates either positions at the times of the gradient pulses or position and velocity, both averaged over the experimental time. Likewise, an experiment employing two gradient pulse pairs (VEXSY) translates into a correlation of initial and final velocity, or velocity with acceleration. One-dimensional versions of the presented experiments can be understood as projections onto the diagonals of the 2D spaces, thus reducing the experimental time at the expense of an information loss about the correlation phenomena. Both techniques were applied to the flow of water through simple geometries (straight cylindrical pipe, and narrowing cylindrical pipe or confusor), and the two-time probability densities of position ($W_2(z_1, 0; z_2, \Delta)$) and velocity ($W_2(v_{z,1}, 0; v_{z,2}, t_m)$) as well as the one-dimensional distribu-

tion functions and correlations derived from them were compared to numerical simulations performed assuming ideal laminar conditions. The experiments demonstrate the feasibility to monitor exchange processes of position, velocity, and perhaps higher order time moments in the Taylor expansion of motion, and of the subsequent analysis process to visualize correlations between different measured quantities. The statistical relations between these quantities are suitable means to describe flow and dispersion processes in more complex geometries and allow applications to systems as diverse as chromatographic columns, porous rocks, and soils as well as capillary structures in plants and in mammal blood vessels. The possibility of stepping **k** space or **q** space at will at two or more separated times bears the potential to extend the conventional concepts of imaging and propagator analysis toward more flexible combinations of multidimensional spatio-temporal-encoding techniques. The experiments and coordinate system presentations suggested in this paper represent one possible realization for this generalized approach of PFG NMR techniques.

REFERENCES

1. P. T. Callaghan, *Rep. Prog. Phys.* **62,** 599 (1999).
2. J. H. Iwamiya, A. W. Chow, and S. W. Sinton, *Rheol. Acta* **33,** 267 (1994).
3. K. Kose, *J. Magn. Reson.* **98,** 599 (1992).
4. J. C. Gatenby and J. C. Gore, *J. Magn. Reson. A* **121,** 193 (1996).
5. K. J. Packer and J. J. Tessier, *Mol. Phys.* **87,** 267 (1996).
6. J. J. Tessier, K. J. Packer, J.-F. Thovert, and P. M. Adler, *AIChE J.* **43,** 1653 (1997).
7. J. J. Tessier and K. J. Packer, *Phys. Fluids* **10,** 75 (1998).
8. L. Lebon, L. Oger, J. Leblond, J. P. Hulin, N. S. Martys, and L. M. Schwartz, *Phys. Fluids* **8,** 293 (1996).
9. L. Lebon, J. Leblond, and J. P. Hulin, *Phys. Fluids* **9,** 481 (1997).
10. M. H. G. Amin, S. J. Gibbs, R. J. Chorley, K. S. Richards, T. A. Carpenter, and L. D. Hall, *Proc. R. Soc. London A* **453,** 489 (1997).
11. J. D. Seymour and P. T. Callaghan, *AIChE J.* **43,** 2096 (1997).
12. R. S. Maier, D. M. Kroll, Y. E. Kutsovsky, H. T. Davis, and R. S. Bernard, *Phys. Fluids* **10,** 60 (1998).
13. U. Tallarek, D. van Dusschoten, H. Van As, E. Bayer, and G. Guiochon, *J. Phys. Chem. B* **102,** 3486 (1998).
14. B. Manz, P. Alexander, and L. F. Gladden, *Phys. Fluids* **11,** 259 (1999).
15. J. Kärger and W. Heink, *J. Magn. Reson.* **51,** 1 (1983).
16. S. Stapf, K. J. Packer, R. G. Graham, J.-F. Thovert, and P. M. Adler, *Phys. Rev. E* **58,** 6206 (1998).
17. S. Stapf and K. J. Packer, *Appl. Magn. Reson.* **15,** 303 (1998).
18. S. Stapf, K. J. Packer, S. Békri, and P. M. Adler, *Phys. Fluids* **12,** 566 (2000).
19. V. Göbbels, "Zweidimensionale Magnetische Resonanz an porösen Medien," Dissertation, RWTH Aachen (1999).
20. B. Blümich, P. Blümler, L. Gasper, A. Guthausen, V. Göbbels, S. Laukemper-Ostendorf, K. Unseld, and G. Zimmer, *Macromolec. Symp.* **141,** 83 (1999).
21. P. P. Mitra, *Phys. Rev. B* **51,** 15074 (1995).
22. S. Stapf, R. A. Damion, and K. J. Packer, *J. Magn. Reson.* **137,** 316 (1999).
23. P. T. Callaghan and B. Manz, *J. Magn. Reson. A* **106,** 260 (1994).
24. P. T. Callaghan, S. L. Codd, and J. D. Seymour, *Concepts Magn. Reson.* **11,** 181 (1999).
25. P. T. Callaghan, "Principles of Nuclear Magnetic Resonance Microscopy," Clarendon Press, Oxford (1991).
26. B. Blümich, "NMR Imaging of Materials," Oxford Univ. Press, Oxford (2000).
27. S. Han and B. Blümich, *Appl. Magn. Reson.* **18,** 101 (2000).
28. J. M. Pope and S. Yao, *Concepts Magn. Reson.* **5,** 281 (1993).
29. O. Reynolds, *Phil. Trans. R. Soc. London* **174,** 935 (1883).
30. P. T. Callaghan and Y. Xia, *Makromol. Chem. Macromol. Symp.* **34,** 277 (1990).
31. T.-Q. Li, J. D. Seymour, R. L. Powell, M. J. McCarthy, K. L. McCarthy, and L. Ödberg, *AIChE J.* **40,** 1408 (1994).
32. S. L. Codd, B. Manz, J. D. Seymour, and P. T. Callaghan, *Phys. Rev. E* **60,** R3491 (1999).